INTERNATIONAL JOURNAL FOR NUMERICAL METHODS IN FLUIDS
Int. J. Numer. Meth. Fluids 2002; **40**:669–695 (DOI: 10.1002/fld.369)

Numerical study of flows of complex fluids between eccentric cylinders using transformation functions

Dana Radu Grecov[1] and Jean-Robert Clermont[2,*,†]

[1] *University Politechnica of Bucarest, Department of Mechanics of Precision, Faculty of Mechanics, Splaiul Independentei, No 313, Bucarest, Romania*
[2] *Laboratoire de Rhéologie UMR 5520 CNRS, Université Joseph-Fourier, Institut National Polytechnique de Grenoble, Domaine Universitaire, B.P. No. 53, 38041 Grenoble Cedex 9, France*

SUMMARY

In this paper, we investigate fluid flows between eccentric cylinders by means of two stream-tube analyses. The first method considers a one-to-one global transformation function that allows the physical domain to be transformed into a mapped domain, used as computational domain, that involves concentric streamlines. The second approach uses local transformations and domain decomposition techniques to deal with mixed flow regimes. Both formulations are particularly adapted for handling time-dependent constitutive equations, since particle-tracking problems are avoided. Mass conservation is verified in both formulations and the relevant numerical procedure can be carried out using simple meshes built on the mapped streamlines. Fluids obeying anelastic and viscoelastic constitutive equations are considered in the calculations. The numerical results are consistent with those in the literature for the flow rates tested. Application of the method to the K-BKZ memory-integral constitutive equation highlights significant differences between the model predictions and those provided by more simple rheological models.

KEY WORDS: domain decomposition; mapping functions; journal bearing; eccentric rotating cylinders; viscoelasticity; time-dependent equations; stream-tube method

1. INTRODUCTION

Numerous studies have been devoted to flows in the annulus of eccentric cylinders, generally related to lubrication problems occurring in journal bearings [1–15]. The growing interest in considering materials with non-Newtonian properties in lubrication [6, 7, 10] has led to generate various numerical techniques being formulated for investigating such flows with complex constitutive equations, where experimental, mathematical and computational techniques are concerned.

* Correspondence to: J.-R. Clermont, Laboratoire de Rhéologie UMR 5520 CNRS, Université Joseph-Fourier, Institut National Polytechnique de Grenoble, B.P. 53, 38041 Grenoble Cedex 9, France.
† E-mail: clermont@ujf-grenoble.fr

Received December 2000
Revised March 2002

Various methods, involving notably spectral approaches, have been developed in the literature in order to simulate flows of fluids obeying complex constitutive equations in eccentric geometries. Formerly, analytical methods were used to determine the flow characteristics, as done for example by Phan-Thien and Tanner [8], who proposed an asymptotic method to evaluate non-Newtonian effects in a journal bearing. Davies and Li [9] adopted a pseudospectral method with bipolar transformation to simulate non-isothermal flows between eccentrically rotating cylinders, using a White–Metzner viscoelastic differential model for the fluid. Gwynllyw and Phillips [11] proposed preconditioned iterative methods for calculating unsteady flows of generalized Newtonian fluids between eccentric cylinders by spectral element calculations. Beris *et al.* [12, 13] have studied steady flows between slightly eccentric cylinders, using anelastic (Newtonian, second-order fluid) as well as viscoelastic differential models, where a Galerkin finite-element method and a spectral finite-element technique were applied. Similarly, the analysis proposed by Chawda *et al.* [14] involved numerical pseudospectral methods to compute steady-state flow between eccentric rotating cylinders and to explore the stability of three-dimensional disturbances, for an upper-convected Maxwell fluid. A spectral element approach has been recently proposed by Li *et al.* [15] in order to investigate specific lubrication problems related to the separate and combined effects of shear-thinning, temperature-thinning and temperature-thickening in two-dimensional journal bearings.

Despite the significant numerical effort to simulate flows of viscoelastic fluids in eccentric geometries, we are not aware, at the present time, of such flow calculations with memory-integral constitutive equations. This situation can probably be explained by difficulties arising when the kinematic tensors and stresses on pathlines have to be evaluated. As pointed out by many authors [16, 17], such quantities based on relative deformation gradients require very accurate estimates for particles on their streamlines (or pathlines) that generally do not pass through the mesh nodes defined in the discretization procedure.

One of the main objectives of this paper is to apply analyses based on stream-tube methods [18–21] that may enable flows of incompressible fluids obeying time-dependent constitutive equations to be simulated using simple computational domains. Calculations, corresponding here to steady and isothermal situations, are related to two different formulations where transformations of the physical flow domain Ω are concerned. The first approach enables flow computations in a mapped domain Ω^*, where the streamlines (or pathlines) are concentric circles, by means of an unknown global transformation to be determined numerically. Such a method is limited to pure circulating flows in eccentric geometries. The second formulation provides possibilities to compute main flow zones as well as vortex regions using domain decomposition and local transformation functions. Some properties related to the former global method are verified by the local approach, particularly those concerning the simplicity of handling memory-integral constitutive equations. So, the additional geometrical elements allow computation of a general flow field by still considering the concepts of streamlines and stream tubes. Both analyses are expected to permit accurate calculations of annular flows for various constitutive equations, including notably time-dependent models, with spatial variables in a simple computational domain. The fluids, assumed to be incompressible, are investigated under steady and isothermal conditions. The inner cylinder C_0, of radius r_0, rotates with an angular velocity ω. The outer cylinder C_1, of radius r_1, is at rest. The parameter e denotes the distance between the axes of the cylinders. The eccentricity is defined as $\varepsilon = e/(r_1 - r_0)$.

This paper is organized as follows. Firstly, the basic equations of the two formulations to be applied to flow between rotating cylinders are presented with specific developments

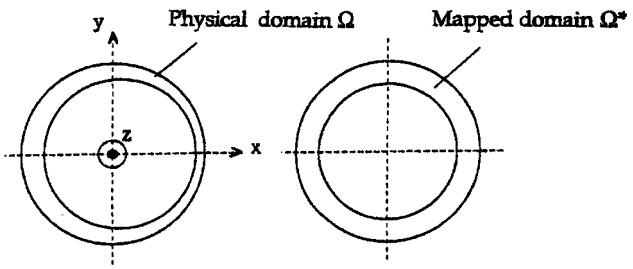

Figure 1. Physical and mapped domains Ω and Ω^* for the two-dimensional flow between eccentric cylinders, with a global transformation function.

relevant to the use of time-dependent constitutive equations. Different complex rheological models are proposed. Next, a specific approach is presented for evaluating kinematic quantities related to moving particles in the flow, for the use of memory-integral constitutive equations. The computational procedure, defined to solve the governing equations, is then applied to annular flows, with and without recirculation, for various eccentricities and rheological models. The numerical results are compared to existing data in the literature and computed solutions relevant to a memory-integral constitutive equation are presented.

2. BASIC EQUATIONS FOR GLOBAL TRANSFORMATIONS OF THE PHYSICAL DOMAIN

This section depicts an analysis similar to the method already presented for flows involving open streamlines such as duct flows [19, 20] and free surface flows [21]. Such cases have concerned transformed domains where the mapped streamlines are parallel and straight. Pure recirculating flows, already suggested in a previous paper [19], have been investigated in a recent study (Radu, PhD Thesis [23]) and are now considered for a plane physical domain Ω shown in Figure 1, referred to Cartesian co-ordinates ($x^1 = x,\ x^2 = y,\ x^3 = z$). The annular domain Ω^* between the two concentric circles of Figure 1 is related to co-ordinates (X^1, X^2, X^3) such that $X^1 = R$; $X^2 = Z$; $X^3 = \Phi$. A transformation $T : (X^1, X^2, X^3) \rightarrow (x^1, x^2, x^3)$ between domains Ω^* and Ω may be defined by the following equations:

$$x = a + R\Lambda(R, \Phi)\cos\Phi; \quad y = b + R\Lambda(R, \Phi)\sin\Phi; \quad z = Z \tag{1}$$

The function $\Lambda(R, \Phi)$ is unknown and the mapped streamlines of domain Ω^* are assumed to be concentric circles. The transformation T is assumed to be one-to-one provided its Jacobian J, given by

$$J = \left| \frac{\partial(x, y, z)}{\partial(R, Z, \Phi)} \right| = R\Lambda(\Lambda + R\Lambda'_R) = \Delta_1 \tag{2}$$

(with $R \neq 0,\ \Lambda \neq 0$) is non-zero. This corresponds to the non-existence of circulatory flow regions. The mapping function Λ must be determined numerically, using Ω^* as the computational domain.

The differential operators $\partial/\partial x, \partial/\partial y, \partial/\partial z$ may be expressed in terms of (R, Z, Φ) by the following relations:

$$\begin{aligned}
\frac{\partial}{\partial x} &= \left[\frac{1}{R\lambda(\Lambda + R\Lambda'_R)}\right]\left[R(\Lambda'_\Phi \cos\Phi - \Lambda\sin\Phi)\frac{\partial}{\partial R} + (\Lambda\cos\Phi + R\Lambda'_R\cos\Phi)\frac{\partial}{\partial\Phi}\right] \\
\frac{\partial}{\partial z} &= \frac{\partial}{\partial Z} \\
\frac{\partial}{\partial y} &= \left[\frac{1}{R\Lambda(\Lambda + R\Lambda'_R)}\right]\left[R(\Lambda'_\Phi \sin\Phi + \Lambda\cos\Phi)\frac{\partial}{\partial R} - (\Lambda\sin\Phi + R\Lambda'_R\sin\Phi)\frac{\partial}{\partial\Phi}\right]
\end{aligned} \tag{3}$$

Using now two Cartesian variables (x^1, x^2), in conditions of infinite journal bearings, such that $\mathbf{x} = x^1\mathbf{e}_1 + x^2\mathbf{e}_2$, we may write the natural basis vectors as [19]

$$\begin{aligned}
\mathbf{b}_1 &= \frac{\partial\mathbf{x}}{\partial R} = \frac{1}{\Delta_1}[(R\Lambda'_\Phi\cos\Phi - R\Lambda\sin\Phi)\mathbf{e}_R + (\Lambda\cos\Phi + R\Lambda'_R\cos\Phi)\mathbf{e}_\Phi] \\
\mathbf{b}_2 &= \frac{\partial\mathbf{x}}{\partial\Phi} = \frac{1}{\Delta_1}[(R\Lambda'_\Phi\sin\Phi - R\Lambda\cos\Phi)\mathbf{e}_R + (\Lambda\sin\Phi + R\Lambda'_R\sin\Phi)\mathbf{e}_\Phi]
\end{aligned} \tag{4}$$

By defining a stream function $\Psi(x, y)$, the velocity components are $u = -\partial\Psi/\partial y$; $v = \partial\Psi/\partial x$. Let us consider in the mapped domain Ω^* a reference section at $\Phi = \Phi_0$, where we put

$$\Psi(R, \Phi_0) = \Psi^*(R) \tag{5}$$

Using Equations (3) and assumptions concerning streamlines in the mapped domain Ω^*, the velocity components, in terms of the variables (R, Φ), become

$$\begin{aligned}
u &= -\frac{1}{\Delta_1}[R(\Lambda'_\Phi\sin\Phi + \Lambda\cos\Phi)]\frac{\mathrm{d}\Psi^*(R)}{\mathrm{d}R} \\
v &= \frac{1}{\Delta_1}[R(\Lambda'_\Phi\cos\Phi - \Lambda\sin\Phi)]\frac{\mathrm{d}\Psi^*(R)}{\mathrm{d}R}
\end{aligned} \tag{6}$$

The function $\Psi^*(R)$ of Equations (5)–(6) may be considered as the mapped stream function related to a streamline in Ω^*. The expression of the velocity vector $\mathbf{V}$ in the basis $(\mathbf{b}_1, \mathbf{b}_2)$ is then readily given by

$$\mathbf{V} = \beta_1(R, \Phi)\mathbf{b}_1 = \left\{\left[\frac{(\Lambda'_\Phi\sin 2\Phi + \Lambda\cos 2\Phi)}{\Lambda\Delta_1}\right]\frac{\mathrm{d}\Psi^*(R)}{\mathrm{d}R}\right\}\mathbf{b}_1 \tag{7}$$

The velocity components of Equation (6) verify the incompressibility condition, thus satisfying conservation of mass.

2.1. Basis vectors related to curvilinear co-ordinates

Owing to the geometrical characteristics of the physical flow domain Ω, we adopt the cylindrical co-ordinates $(r = 1, \theta = 2)$ of the orthonormal basis $\mathbf{c}_i$, allowing the curvilinear co-ordinates $(R = 1, \Phi = 2)$ of domain Ω^* to be related by means of an unknown mapping function λ

such that

$$r = \lambda(R, \Phi); \quad \theta = \Phi \tag{8}$$

The natural basis $\mathbf{b}_i$ can be expressed by the following equations:

$$\begin{aligned} \mathbf{b}_1 &= \lambda'_R \mathbf{c}_1 \\ \mathbf{b}_2 &= \lambda'_\Phi \mathbf{c}_1 + \lambda \mathbf{c}_2 \end{aligned} \tag{9}$$

Using the Jacobian $\Delta = |\partial(R, \Phi)/\partial(r, \theta)|$, the reciprocal vectors χ^1, χ^2 can be written in terms of the basis vectors $\mathbf{c}^i$ as

$$\begin{aligned} \chi^1 &= \frac{1}{\lambda\Delta}(\lambda \mathbf{c}_1 - \lambda'_\Phi \mathbf{c}_2) \\ \chi^2 &= \frac{1}{\lambda\Delta}(\lambda'_R \mathbf{c}_2) \end{aligned} \tag{10}$$

Thus, the metric tensors defined by

$$\begin{aligned} G_{ij}^{-1} &= \mathbf{b}_i \mathbf{b}_j \\ G^{kl} &= \chi^k \chi^1 \end{aligned} \tag{11}$$

may be expressed by the following matrices related to $\mathbf{b}_i$:

$$\begin{aligned} [G^{-1}] &= \begin{pmatrix} (R\lambda'_R + \lambda)^2 & R\lambda'_\phi(R\lambda'_R + \lambda) \\ R\lambda'_\phi(R\lambda'_R + \lambda) & R\lambda'_\phi + R^2\lambda^2 \end{pmatrix} \\ [G] &= \begin{pmatrix} \left(\dfrac{\lambda'\phi^2}{\lambda^2} + 1\right)\dfrac{1}{(R\lambda'_R + \lambda)^2} & -\dfrac{R\lambda'_\phi}{(R\lambda'_R + \lambda)R^2\lambda^2} \\ -\dfrac{R\lambda'\phi}{(R\lambda'_R + \lambda)R^2\lambda^2} & \dfrac{1}{R^2\lambda^2} \end{pmatrix} \end{aligned} \tag{12}$$

2.2. *Particle tracking*

According to the one-dimensional velocity equation (7), the movement versus time of a particle X occupying respective positions $M(R, \Phi)$ and $M_0(R, \Phi_0)$ at times t and t_0 (reference time) is given by

$$t - t_0 = \int_{\Phi_0}^{\Phi} \frac{\mathrm{d}s}{\beta_1(R, s)} \tag{13}$$

This simple equation is written for circular mapped streamlines of domain Ω^*. Such a property avoids the difficulties associated with particle tracking, usually encountered with time-dependent constitutive equations.

2.3. Dynamic equations

Ignoring body forces, the momentum conservation equation (steady-flow conditions) is given by

$$\nabla\tilde{\sigma} = \rho\mathbf{V}\cdot\nabla\mathbf{V} \tag{14}$$

where ρ denotes the fluid density and $\tilde{\sigma}$ the total stress tensor written as

$$\tilde{\sigma} = -p\tilde{I} + \tilde{T} \tag{15}$$

where p denotes the pressure and $\tilde{T}$ is the extra-stress tensor given by the constitutive equation. The two first-order partial differential equations derived from Equation (14) may be expressed in terms of the pressure p, the stress components T^{ij} and the velocities involved in the term $\rho\mathbf{V}\cdot\nabla\mathbf{V}$. By eliminating the pressure, these two equations are reduced into one second-order differential equation as

$$\begin{aligned}&\frac{\partial_2 T_{xx}}{\partial y\,\partial x} + \frac{\partial_2 T_{xy}}{\partial y_2} - \frac{\partial_2 T_{yy}}{\partial x\,\partial y} - \frac{\partial_2 T_{xy}}{\partial x_2}\\ &\quad=\rho\left(v_x\frac{\partial_2 v_x}{\partial y\,\partial x} + v_y\frac{\partial_2 v_x}{\partial y_2} + \frac{\partial v_x}{\partial y}\frac{\partial v_x}{\partial x} + \frac{\partial v_y}{\partial y}\frac{\partial v_x}{\partial y} - v_x\frac{\partial_2 v_y}{\partial x_2}\right.\\ &\qquad\left.-v_y\frac{\partial_2 v_y}{\partial x\,\partial y} - \frac{\partial v_x}{\partial x}\frac{\partial v_y}{\partial x} - \frac{\partial v_y}{\partial x}\frac{\partial v_x}{\partial y}\right)\end{aligned} \tag{16}$$

In Equation (16), v_x and v_y denote the components of the velocity vector $\mathbf{V}$ in Cartesian co-ordinates.

For computational purposes, the different quantities of Equation (16) are expressed in terms of variables (R,Φ) of mapped domain Ω^*, using derivative operators given by Equations (3) [21].

3. BASIC EQUATIONS FOR LOCAL TRANSFORMATIONS

3.1. Transformation of sub-domains

To compute mixed regime flows in the annulus domain Ω, we now consider sub-regions Ω_i that may involve open or closed elementary stream tubes or both. General features of this approach have been presented elsewhere [23]. Figure 2(a) illustrates a sub-domain Ω_m of Ω limited by two azimuth sections defined at angles θ_m and θ_{m+1} $(m=1,2,\ldots,m_0)$ in the eccentric annulus geometry. The m_0 non-overlapping sub-domains Ω_m are defined such that

$$\Omega = \bigcup_{m=1}^{m=m_0}\Omega_m \tag{17}$$

These sub-domains may involve open and closed stream tubes, *a priori* unknown, of the total flow domain Ω. We select, in each sub-domain Ω_m, a reference azimuth section S_m, where $\theta=\theta_{0m}$ (Figure 2(a)).

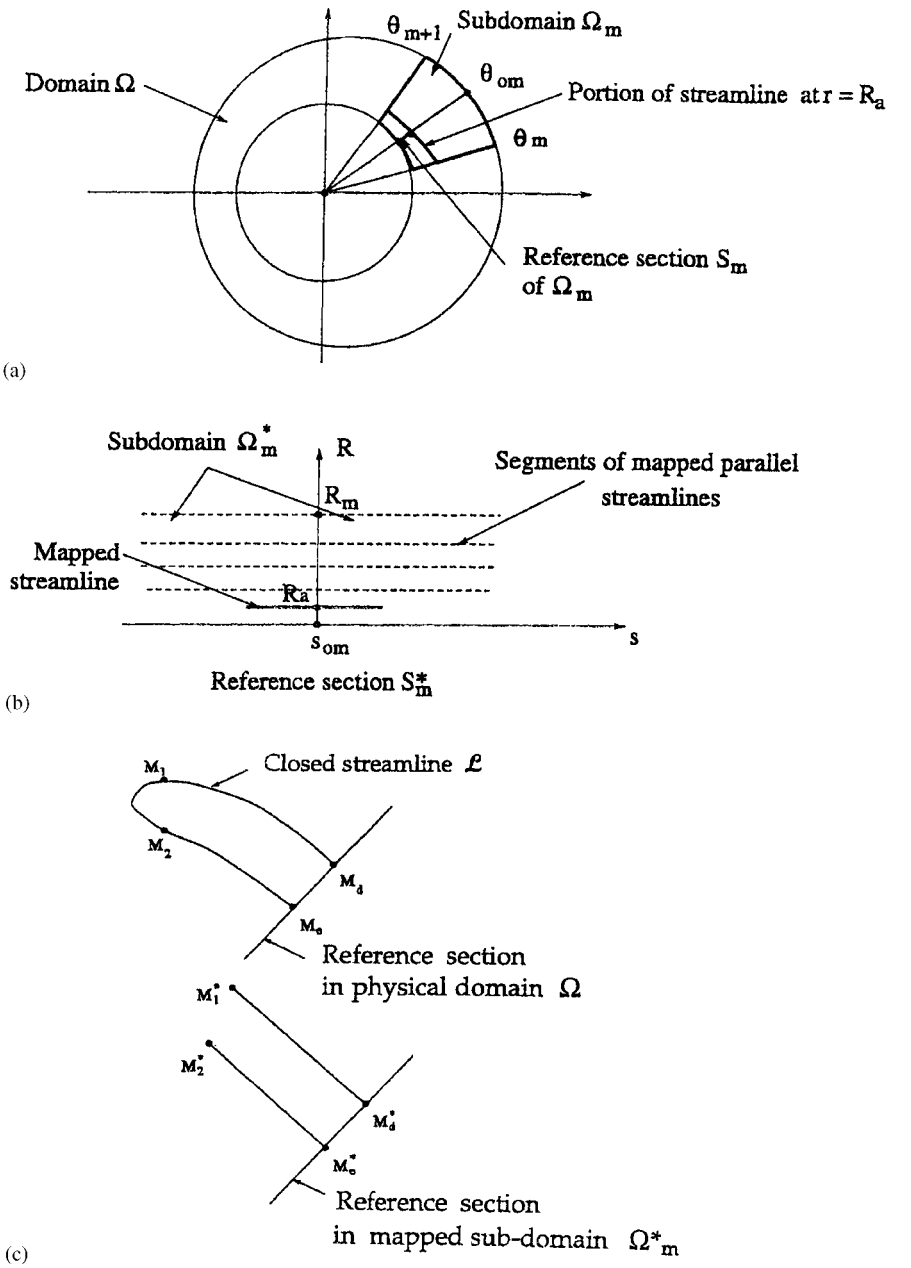

Figure 2. Local transformation functions: (a) sub-domain Ω_m of Ω in the eccentric annulus geometry, involving a reference section S_m; (b) corresponding mapped domain Ω_m^* for the local transformation; (c) geometrical elements for a closed streamline L of sub-domain Ω_m partitioned into two segments in mapped domain Ω_m^*.

Let $(x^1,x^2)_m$ be the local polar co-ordinates in sub-domains Ω_m of Ω defined with respect to the reference flow section S_m. Using a reference section S_m^* identical in shape to S_m, we denote by Ω_m^* the corresponding sub-domain of Ω_m where the mapped streamlines are parallel to a given direction (Figure 2(b)). Sub-domain Ω_m^* is referred to a co-ordinate system ξ^j expressed by

$$\xi^1 = s; \quad \xi^2 = R \tag{18}$$

We define local one-to-one transformations $T_m : (x^1,x^2) \to (\xi^1,\xi^2)$ involving unknown local functions $\alpha(s,R)$ and $\beta(s,R)$ (or $\lambda_1(s,R)$ and $\lambda_2(s,R)$) such that

$$r = \alpha(s,R) = \lambda_1(s,R)R; \quad \theta = \beta(s,R) = \lambda_2(s,R)s/R \tag{19}$$

The co-ordinate R corresponds to the radius r at the reference section $S_m^*(s_0,R)$ of sub-domain Ω_m^*. The co-ordinate s is defined in relation to the curvilinear abscissa χ of a moving particle on its streamline, given by

$$\chi = \chi_0 + \int_{t_0}^{t} |\mathbf{V}(\tau)|\, \mathrm{d}\tau \tag{20}$$

where χ_0 denotes the abscissa corresponding to the reference section S_m^* of the mapped sub-domain Ω_m^* and $|\mathbf{V}(\tau)|$ the modulus of the velocity vector $\mathbf{V}$ on the streamline points. In Equation (20), the times t_0 and t are associated with positions s_0 and s of a material point, respectively.

Defining by s_M $(s_M < +\infty)$ the given total length of a streamline L, originating at a point M_0, in a sub-domain Ω_m and by χ_M $(\chi_M < +\infty)$ the corresponding maximum curvilinear abscissa, we may define the variable s by the following relationship:

$$s = (\chi/\chi_M)s_M \tag{21}$$

In order to express the variable s for a streamline L of zero velocity (presence of a wall where the fluid adheres), the co-ordinate χ related to a point M is assumed to be the curvilinear distance $\mathbf{M_0M}$.

Figure 2(c) illustrates the case of a closed streamline L belonging to a sub-domain Ω_m, intersecting the reference section S_m at points M_d and M_e. In the corresponding mapped domain Ω_m^*, this transformed streamline is partitioned into two different segments originating at points M_d^* and M_e^*, the respective transformed points of M_d and M_e at the mapped reference section S_m^*. Accordingly, the two points M_1 and M_2 of the streamline L are associated with transformed points M_1^* and M_2^* of two different segments.

The one-to-one assumption for the local transformations T_m implies that the Jacobian Δ expressed by

$$\Delta = \det|\partial(x^i)/\partial(\xi^j)| = \alpha'_s\beta'_R - \alpha'_s\beta'_R \tag{22}$$

is non-zero. In Equation (22), α'_s, β'_R, α'_s and β'_R denote the partial derivatives in terms of variables s and R. Derivative operators relating the co-ordinates (r,θ) to the new system of local co-ordinates (s,R) are thus given by

$$\begin{aligned} \partial/\partial r &= 1/\Delta[\beta'_R\partial/\partial s - \beta'_s\partial/\partial R] \\ \partial/\partial\theta &= 1/\Delta[\alpha'_R\partial/\partial s - \alpha'_s\partial/\partial R] \end{aligned} \tag{23}$$

Given a point $M^*(s,R)$ of Ω_m^*, the unit vectors $\mathbf{c}_i$ related to cylindrical co-ordinates (r,θ) can be expressed in terms of the natural basis $(\mathbf{g}_s,\mathbf{g}_R)$ (with $s=1,\ R=2$) according to the relations

$$\mathbf{c}_1=(1/\Delta)[\beta'_s\mathbf{g}_s-\beta'_R\cdot\mathbf{g}_R];\quad \mathbf{c}_2=(1/\Delta)[\alpha'_s\mathbf{g}_s-\alpha'_R\cdot\mathbf{g}_R] \tag{24}$$

Conversely, we also obtain the equations

$$\mathbf{g}_s=\alpha'_s\mathbf{c}_1+\alpha\beta'_s\mathbf{c}_2;\quad \mathbf{g}_R=\alpha'_R\mathbf{c}_1+\alpha\beta'_R\mathbf{c}_2 \tag{25}$$

and hence the reciprocal basis vectors $(\mathbf{g}^s,\mathbf{g}^R)$ can be written as

$$\begin{aligned}\mathbf{g}^s &= [1/(\alpha\Delta)][\alpha\beta'_R\mathbf{c}_1-\alpha'_R\mathbf{c}_2]\\ \mathbf{g}^R &= [1/(\alpha\Delta)][-\alpha\beta'_s\mathbf{c}_1+\alpha'_s\mathbf{c}_2]\end{aligned} \tag{26}$$

From these expressions, the matrices of metric tensors given by $G_{sR}^{-1}=[\mathbf{g}_s\cdot\mathbf{g}_R]$ and $G^{sR}=[\mathbf{g}^s\cdot\mathbf{g}^R]$ can be written as

$$G=\begin{bmatrix} G^{ss} & G^{sR}\\ G^{Rs} & G^{RR}\end{bmatrix} \tag{27}$$

of components

$$\begin{aligned}G_{ss} &= (\alpha'_s)^2+\alpha^2(\beta'_s)^2;\quad G_{Rs}=G_{sR}=\alpha'_s\alpha'_R+\alpha^2\beta'_s\beta'_R\\ G_{RR} &= (\alpha'_R)^2+\alpha^2(\beta'_R)^2\end{aligned} \tag{28}$$

and

$$\lambda^0=\sum_p(a_p\lambda_p^2)/\sum_p(a_p\lambda_p),\quad p=1,2,3 \tag{29}$$

of components

$$\begin{aligned}G^{ss} &= [1/\Delta^2][(\beta'_R)^2+(\alpha'_R/\alpha)^2]\\ G^{sR} &= G^{Rs}=[1/\Delta^2][\beta'_R\beta'_s+(\alpha'_R\alpha'_s)/\alpha^2]\\ G^{RR} &= [1/\Delta^2][(\beta'_s)^2+(\alpha'_s/\alpha)^2]\end{aligned} \tag{30}$$

3.2. Kinematic equations and particle tracking

In polar co-ordinates, the velocity component equations written in terms of a stream function $\Psi(r,\theta)$ as $v_r=(1/r)\partial\Psi(r,\theta)/\partial\theta$; $v_\theta=-\partial\Psi(r,\theta)/\partial r$ can be expressed by means of variables (s,R) as

$$\begin{aligned}v_r &= -\{\alpha'_s(s,R)/[\alpha(s,R)\Delta]\}\mathrm{d}\Psi^*(R)/\mathrm{d}R\\ v_\theta &= \{\beta'_s(s,R)/\Delta\}\,\mathrm{d}\Psi^*(R)/\mathrm{d}R\end{aligned} \tag{31}$$

In Equations (31), $\Psi^*(R)$ denotes the transformed stream function of Ψ, written from a reference kinematic function at section S_m^* of co-ordinates (s_0,R) such that

$$\mathrm{d}\Psi^*(R)/\mathrm{d}R=v_\theta(s_0,R)=H^*(R) \tag{32}$$

Since the relevant unknowns of the problem are expected to be determined iteratively, the function $\Psi^*(R)$, *a priori* unknown, must be updated at each step of the procedure. We also postulate the following conditions at the reference section:

$$\alpha'_R(s_0,R)=1; \quad \beta'_s(s_0,R)=0 \tag{33}$$

From Equation (32), the velocity equations (31) become

$$\begin{aligned} v_r &= -\{\alpha'_s(s,R)/[\alpha(s,R)\Delta]\}H^*(R) \\ v_\theta &= -\{\beta'_s(s,R)/\Delta\}H^*(R) \end{aligned} \tag{34}$$

In the flow domain, the co-ordinate θ on a streamline of non-zero velocity can be expressed by the following equation:

$$\theta=\theta_0+H^*(R)\int_{s_0}^{s}[\beta'_s(\xi,R)/\Delta]\,\mathrm{d}\xi \tag{35}$$

Concerning particle tracking for a material point moving on its streamline in a sub-domain Ω_m, the movement versus time is expressed by a relationship similar to Equation (13). The time t_0 is related to the reference sections of domains Ω_m and Ω_m^*.

3.3. Dynamic equations

Ignoring inertia and body forces, we can write the dynamic equations, along the two axes (r,θ) of the physical domain Ω, using the local variables (s,R) of the sub-domain Ω_m under consideration as follows:

$$\begin{aligned} &\alpha[\beta'_s\partial p/\partial R-\beta'_R\partial p/\partial s]+\beta'_s\partial(\alpha T^{rr})/\partial R-\beta'_R\partial(\alpha T^{rr})/\partial s \\ &-\beta'_R\partial(\alpha T^{rr})/\partial s-\alpha'_s\partial(\alpha T^{r\theta})/\partial R+\alpha'_R\partial(T^{r\theta})/\partial s=0 \end{aligned} \tag{36}$$

$$\begin{aligned} &\alpha'_s\partial p/\partial R+\alpha'_s\partial p/\partial s+\beta'_s\partial(\alpha T^{r\theta})/\partial R-\beta'_R\partial(\alpha T^{r\theta})/\partial s \\ &+\alpha'_s\partial(T^{rr})/\partial R-\alpha'_R\partial(T^{rr})/\partial s=0 \end{aligned} \tag{37}$$

4. CONSTITUTIVE EQUATIONS AND SPECIFIC RELATIONS

Several models for inelastic and viscoelastic materials obeying differential and memory-integral equations are adopted in the flow computations.

4.1. Inelastic models

The models retained here correspond to the classic Newtonian fluid and a non-Newtonian purely viscous fluid given by

$$\tilde{T}=\eta(\tilde{D})\tilde{D} \tag{38}$$

where the viscosity η depends on the rate-of-strain tensor $\tilde{D}$. The viscosity function obeys a Carreau law [12] written as

$$\frac{(\eta-\eta_\infty)}{(\eta_0-\eta_\infty)}=\frac{1}{(1+\gamma K^a)^b} \tag{39}$$

In Equation (39), the velocity gradient γ is related to the second invariant $\Pi_{\tilde{D}}$ of $\tilde{D}$ by the equation

$$\gamma=\sqrt{2\Pi_{\tilde{D}}} \tag{40}$$

K denotes a material constant of the fluid and a, b are dimensionless coefficients. η_0 and η_∞ ($\eta_0>\eta_\infty$) are corresponding viscosities at low and high shear rates, respectively.

4.2. Viscoelastic models

4.2.1. Differential models. The constitutive Oldroyd-B equation expresses the extra-stress tensor $\tilde{T}$ according to the following implicit form:

$$\lambda_1\frac{\Delta\tilde{T}}{\Delta t}+\tilde{T}=2\eta_0\left(\tilde{D}+\lambda_2\frac{\Delta\tilde{D}}{\Delta t}\right) \tag{41}$$

where $\Delta/\Delta t$ denotes the upper convected derivative [24] defined for a contravariant symmetric tensor, λ_1 a relaxation time and λ_2 is called the retardation time. The particular case $\lambda_2=0$ gives the upper-convected Maxwell model [24]. For these models, the corresponding viscosity function is a constant.

4.2.2. The integral model. The memory-integral equation adopted here is a time-dependent codeformational K-BKZ model involving multiple relaxation times, of the form proposed by Papanastasiou *et al.* [25]. In our calculations, we used the data provided by Chai and Yeow [26] for a polymer solution, expressing the stress tensor as follows:

$$\tilde{T}(t)=\int_{-\infty}^{t}\sum_{p=1}^{3}\frac{a_p}{\lambda_p}\exp\left(-\frac{(t-t')}{\lambda_p}\right)\frac{\alpha\tilde{B}_{t'}(t)}{\alpha-3+\beta\,\mathrm{tr}\,\tilde{B}+(1-\beta)\,\mathrm{tr}\,\tilde{B}^{-1}}\,\mathrm{d}t' \tag{42}$$

where t denotes the time under consideration, t' a previous time with $t'\leqslant t$, a_p and λ_p are the moduli and corresponding relaxation times, respectively. $\tilde{B}_{t'}$ is the Finger tensor, $\tilde{B}_{t'}^{-1}$ the Cauchy tensor related to the configuration at times t'. α and β denote material constants of the fluid, determined experimentally and are found to be $\alpha=500$ and $\beta=0.001$. The coefficients a_p and λ_p of the model are given in Table I.

4.3. Kinematic quantities for the memory-integral model

The Finger and Cauchy tensors to be considered in the constitutive equation (42) are related to the deformation gradient tensor $\tilde{F}_t(t)=[\partial x_{t'}^m/\partial x_t^\gamma]$ by the following relations [24]:

$$\begin{aligned}\tilde{B}_t(t') &= [{}^T\tilde{F}_t(t')\tilde{F}_t(t')]^{-1}\\ \tilde{B}_t^{-1}(t') &= {}^T\tilde{F}_t(t')\tilde{F}_t(t')\end{aligned} \tag{43}$$

Table I. Numerical data of λ_p and a_p used in the K-BKZ memory-integral equation (after Chai andYeow [24]).

P	λ_p(s)	a_p(Pa)
1	1.04	0.55
2	8.9×10^{-2}	5.46
3	5.2×10^{-4}	3.06×10^{-3}

To evaluate the deformation gradient tensor $\tilde{F}_t(t)$, we start from Adachi's work [27, 28] on Protean co-ordinates [29]. The approach, defined in relation to variables defined in global or local transformation systems, is similar to that previously followed in stream-tube analysis [30, 31] for flows involving open streamlines.

4.3.1. Global transformations. According to the relevant curvilinear co-ordinate system ($\xi^1 = R, \xi^2 = \Phi$) in the mapped domain Ω^*, we can express the deformation gradient tensor as [24]

$$[F^{-1}] = \begin{pmatrix} \partial s/\partial R' & \partial s/\partial s' \\ 1 & 0 \end{pmatrix} \tag{44}$$

with

$$\frac{\partial \Phi}{\partial \Phi'} = \frac{V(R,\Phi)}{V(R,\Phi')} \tag{45}$$

$$\frac{\partial \Phi}{\partial R'} = V(R,\Phi) \int_{\Phi'}^{\Phi} \frac{\partial V}{\partial R}(R,\xi) \frac{\mathrm{d}\xi}{V^2(R,\xi)} = V(R,\Phi) \int_{t'}^{t} \frac{\partial V}{\partial R}(R,\Phi(\tau)) \frac{\mathrm{d}\tau}{V(R,\Phi(\tau))} \tag{46}$$

In Equations (44)–(46), variables (R', Φ') are referred to material positions at times t'. In the present case, we have $R' = R$, according to the circular shape of the mapped streamlines in domain Ω^*.

The Finger tensor components can be written in terms of the metric tensor $\tilde{G}$ in the basis $\mathbf{b}_i$ by the following matrix equation:

$$[B] = [F][G][F]^{\mathrm{T}} \tag{47}$$

with the following components:

$$B_{RR} = G^{R'R'} \tag{48}$$

$$B_{\Phi\Phi} = G^{R'R'} \frac{\partial \Phi}{\partial R'} + G^{R'\Phi'} \frac{\partial \Phi}{\partial \Phi'} \tag{49}$$

$$B_{R\Phi} = \left(\frac{\partial \Phi}{\partial R'}\right)^2 G^{R'R'} + 2 \frac{\partial \Phi}{\partial \Phi'} \frac{\partial \Phi}{\partial R'} G^{\Phi'R'} + \left(\frac{\partial \Phi}{\partial \Phi'}\right)^2 G^{\Phi'\Phi'} \tag{50}$$

Using the matrix of passage $[A]$ from the natural basis $\mathbf{b}_i$ to the cylindrical basis $\mathbf{c}_i$

$$[A] = \begin{pmatrix} f'_R & f g'_R \\ f'_\Phi & f g'_\Phi \end{pmatrix} = \begin{pmatrix} R\lambda'_R & 0 \\ R\lambda'_\Phi & R\lambda \end{pmatrix} \tag{51}$$

the components of $\tilde{B}$ can be written in the cylindrical basis $\mathbf{c}_i$ as

$$B_{rr} = B_{RR}(R\lambda'_R + \lambda)^2 + B_{R\Phi}2(R\lambda'_R + \lambda)R\lambda'_\Phi + (R\lambda'_\Phi)^2 B_{\Phi\Phi} \tag{52}$$

$$B_{r\theta} = B_{R\Phi}(R\lambda'_R + \lambda)R\lambda + B_{\Phi\Phi}R^2\lambda\lambda'_\Phi \tag{53}$$

$$B_{\theta\theta} = B_{\Phi\Phi}(R\lambda)^2 \tag{54}$$

are used to determine the Cauchy tensor components and also the invariants $\mathrm{tr}(\tilde{B})$ and $\mathrm{tr}(\tilde{B}^{-1})$ involved in the integral constitutive equation (42).

Stress calculations for different positions of the material point on its closed streamline are performed by taking into account the periodicity of the flow, related to the angle Φ in the mapped domain Ω^*. The tensor components are then evaluated for points M^* of the circular mapped streamlines by six-point Gauss–Laguerre formulae.

4.4. Local transformations

The approach is quite similar to that followed for global transformations. The use of co-ordinates $s = 1$ and $R = 2$ means writing the deformation gradient term in the following matrix form, in the curvilinear basis $(\mathbf{g}_s \cdot \mathbf{g}_R)$ [23]:

$$[F^{-1}] = \begin{pmatrix} \partial s/\partial R' & \partial s/\partial s' \\ 1 & 0 \end{pmatrix} \tag{55}$$

where (s, R) and (s, R') correspond to material positions at times t and t', respectively, with $R = R'$. Similar Equations (49)–(50), we obtain

$$\begin{aligned} \partial s/\partial s' &= v_s(s,R)/v_s(s',R) \\ \partial s/\partial R' &= v_s(s,R)\int_{t'}^{t} \partial[v_s(s(\tau),R)]/\partial R \,\mathrm{d}\tau / v_s(s(\tau),R) \end{aligned} \tag{56}$$

According to Equation (40), the Finger tensor components expressed in a matrix form as

$$[A] = \begin{bmatrix} \alpha'_s & \alpha\beta'_s \\ \alpha'_R & \alpha\beta'_R \end{bmatrix} \tag{57}$$

are given by the following relations:

$$\begin{aligned} B_{ss} &= (\partial s/\partial s')^2 G^{s's'} + 2(\partial s/\partial s')(\partial s/\partial R')G^{s'R'} + (\partial s/\partial R')2G^{R'R'} \\ B_{sR} &= B_{Rs} = (\partial s/\partial s')G^{s's'} + (\partial s/\partial R')G^{s'R'} \\ B_{RR} &= G^{s's'} \end{aligned} \tag{58}$$

The matrix of change from the natural basis at time t to the cylindrical basis is given by

$$[A] = \begin{bmatrix} \alpha'_s & \alpha\beta'_s \\ \alpha'_R & \alpha\beta'_R \end{bmatrix} \tag{59}$$

The matrix form of the Finger tensor in the cylindrical basis $\mathbf{c}_i$ of the physical domain can then be expressed by

$$[B]\mathbf{c}_i = {}^{\mathrm{T}}[A][B]\mathbf{g}_i[A] \tag{60}$$

Thus we get the following components:

$$\begin{aligned} B_{rr} &= (\alpha'_s B_{ss} + \alpha'_R B_{sR})\alpha'_s + (\alpha'_R B_{RR} + \alpha'_s B_{sR})\alpha'_R \\ B_{r\theta} &= (\alpha'_s B_{ss} + \alpha'_R B_{sR})\alpha\beta'_s + (\alpha'_s B_{sR} + \alpha'_R B_{RR})\alpha\beta'_R \\ B_{\theta\theta} &= (\alpha\beta'_s B_{ss} + \alpha\beta'_R B_{sR})\alpha\beta'_s + (\alpha\beta'_s B_{sR} + \alpha\beta'_R B_{RR})\alpha\beta'_R \end{aligned} \tag{61}$$

The Cauchy tensor can be evaluated from the Finger tensor components.

5. NUMERICAL PROCEDURE AND RESULTS

The governing equations involve the dynamic and constitutive equations, together with boundary condition relations. Mass conservation is verified by both analyses. We adopted a mixed formulation where the unknowns are the pressure, the mapping functions and the stress components T_{ij}. Owing to symmetry properties, we consider the half-domain Ω of the annulus geometry. The code, related to pure circulating and mixed regime flow conditions, was implemented on a work station (Pentium 333 MHz processor). Tests were performed for inelastic (Newtonian and purely viscous Carreau) fluids and viscoelastic materials modelled by differential equations, for which comparisons with data from the literature were possible. The inertial terms of the momentum equations were involved in the calculations and, as expected, were found to be negligible at low velocity gradients. As flow parameters, we used the Reynolds number $Re = \rho r_0 \omega/\eta$ and, for viscoelastic fluids, the Weissenberg number [11] We given by

$$We = \lambda^0 \omega \tag{62}$$

where λ^0 denotes a characteristic time. According to Luo and Tanner [17], we adopted for the multimode K-BKZ equation (42) a mean relaxation time, expressed by the following relation:

$$\lambda^0 = \sum_p (a_p \lambda_p^2) / \sum_p (a_p \lambda_p), \quad p = 1, 2, 3 \tag{63}$$

The parameter λ^0 was found to be 0.6.

We also define the following ratio E of the Weissenberg and Reynolds numbers as

$$E = We/Re \tag{64}$$

5.1. Procedure and results for global transformations

When using a global transformation function λ, the mapped domain Ω^* is rectangular, with variables R $(0 \leqslant R \leqslant R_a = r_1 - r_0)$ and Φ, for $0 \leqslant \Phi \leqslant \pi$. The segments C_0^* and C_1^* are the

transformed lines of the curves C_0 and C_1 of the cylinders, respectively. The reference section at $\Phi = 0$ adopted to define the function Ψ^* (Equation (5)) is taken at $\Phi = 0$.

The conditions for the global function λ on the mapped boundaries C_0^* and C_1^*, the respective transformed lines of the curves C_0^* and C_1^* are

$$\lambda = e\cos\Phi + \sqrt{e^2\cos^2\Phi - e^2 + r_0} \quad \text{for } C_0^* \tag{65}$$

and

$$\lambda = r_1 \quad \text{for } C_1^* \tag{66}$$

The 2π-periodicity condition in terms of the variable Φ for all the unknowns is also necessary.

The values of the function Ψ^* (Equation (5)) at the reference section $\Phi = 0$ are *a priori* unknown. This function needs to be evaluated iteratively. Its initial estimate was provided by the Couette solution for the velocities, using the equation

$$R \in [0{:}\, R_a]{:}\;\; \Psi^*(R) = \int_0^R v_\Phi(\xi)\xi \,\mathrm{d}\xi \tag{67}$$

For the next iterations, the function Ψ^* was updated using the same Equation (64). The next value of λ allowed a new iterate of the v_Φ-velocity component to be computed.

A rectangular grid, refined in the vicinity of the reference section $\Phi = 0$ in the Φ-direction, but uniform in the R-direction, was defined in domain Ω^* to discretize the unknowns and equations. Typically, the grid used for the computations involved 30×30 mesh points. Finite-difference formulae were adopted to approximate the derivatives involved in the equations. Thus, the set of discretized governing and boundary condition equations may be written as

$$A_j(X_1, X_2, \ldots, X_N) = 0, \;\; i = 1, 2, \ldots, N \tag{68}$$

where $(X_1, X_2, \ldots, X_N) = \mathbf{X}$ denotes the vector of unknowns. Thus, the following quadratic objective function $S(\mathbf{X})$ can be defined by means of the following matrix product of $\mathbf{A}(\mathbf{X})$ and its transpose ${}^{\mathbf{T}}\mathbf{A}(\mathbf{X})$ such that

$$S(\mathbf{X}) = {}^{\mathbf{T}}\mathbf{A}(\mathbf{X}) \cdot \mathbf{A}(\mathbf{X}) = \sum_{j=1}^{i=N} A_j^2(X_1, X_2, \ldots, X_N) \tag{69}$$

Using the objective function $S(\mathbf{X})$, the unknowns is determined by means of the Levenberg–Marquardt optimization algorithm [32, 33] already used for numerical problems involving stream-tube analysis [20, 21]. This procedure, which combines the Newton and gradient algorithms, proved to be robust and efficient, especially for problems where slight modifications of the unknowns may lead to significant changes in the equations, as in the present case that concerns streamlines as primary variables.

The number of iterations before convergence, in the case of global transformations, was found to be approximately 30 for all the fluids tested. The corresponding CPU time, depending on the type of fluid under consideration, was approximately 7 s per iteration for a Newtonian fluid and reached 210 s for the viscoelastic K-BKZ memory-integral constitutive equation. Different eccentricities and geometrical conditions were considered for various rotation rates of the inner cylinder. Figure 3 reports the evolution of the norm of the objective function $S(\mathbf{X})$

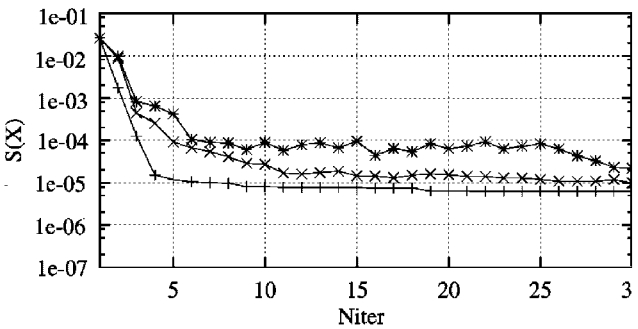

Figure 3. Change in the objective function versus the iteration number for different fluids: $+ + ++$: Newtonian; $\times \times \times\times$: Oldroyd-B (differential); $* * * *$: K-BKZ (integral).

versus the iteration number Niter for different fluids investigated. Better convergence occurs for the Newtonian equation and the differential viscoelastic Oldroyd-B fluid, as compared to the K-BKZ fluid. Such behaviour should be related to non-linearities involved in the differential and integral models, these being more sensitive for the multiple-mode K-BKZ equation.

5.1.1. Appearance of recirculations. Such predictions may be of interest for industrial applications related to flows between eccentric cylinders. From a theoretical viewpoint, the appearance of vortices is related here to the assumptions made on the non-existence of recirculations allowing verification of the one-to-one property concerning streamlines of the physical domain and their mapped streamlines in domain Ω^* the global transformation. Consequently, a divergence of the algorithm was expected for flow parameters close to those related to the appearance of recirculating regions. The convergence of the Newtonian results obtained with our code, reported in Figure 4(a) with those of Diprima *et al.* [1], Chawda *et al.* [14], and Dai *et al.* [34] confirms this theoretical prediction and points out the consistency of our data with results in the literature obtained by different computational approaches. For other fluids, there were no available data in the literature allowing such comparisons. We may conjecture that the non-convergence of our algorithm results from the vanishing of the Jacobian of the global transformation, in a way similar to the conditions for appearance of secondary flows in geometries involving open streamlines, previously investigated in stream-tube computations [19]. For the memory-integral fluid, Figure 4(b) presents a limiting curve between the convergence and divergence zones related to the algorithm, when expressing the Weissenberg number *We* versus the eccentricity. Although results for such fluids were not available in the literature, our opinion is that the separating curve is related to the appearance of recirculating zones in the flow region, as in the Newtonian case.

5.1.2. General results and comparisons. To express the kinematic results, we used the normalized radial co-ordinate r^* given by $r^* = (r - r_0 - e\cos\theta)/[\delta(1 - \varepsilon\cos\theta)]$, $r^* \in [0, 1]$ where $\delta = r - r_0$. The velocity parameter (dimensionless factor) is $v^* = \omega r_0$. Consistent comparisons of azimuthal velocities v_θ between our results and data from the literature [7], for a Newtonian and a purely viscous fluid obeying a Carreau equation, are shown in Figure 5(a) and 5(b), respectively. Figure 6 shows normalized velocity profiles v_θ versus r^* for the three viscoelastic fluids investigated in the present work: Maxwell, Oldroyd-B and K-BKZ at a

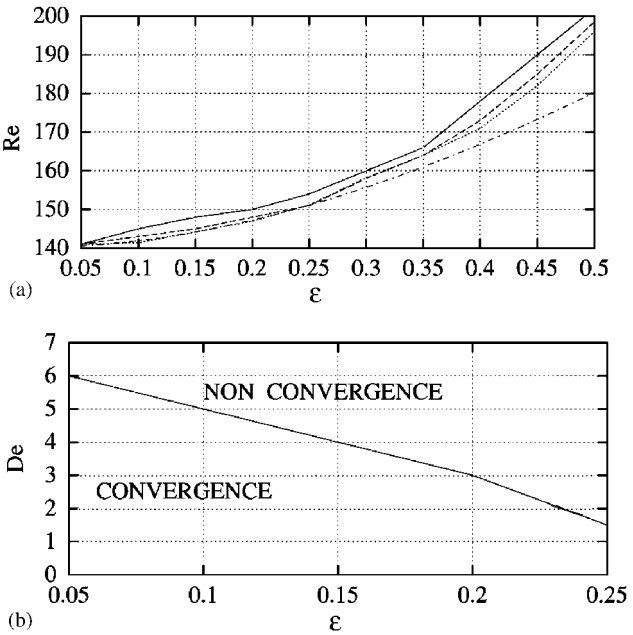

Figure 4. Limit curves for the appearance of recirculations: (a) for a Newtonian fluid, expressing the Reynolds number *Re* as a function of the eccentricity ε: ——: present work; · - · - · -: Diprima *et al.* [1]; - - - -: Chawda *et al.* [14]; · · · · ·: Dai *et al.* [34]; (b) for a memory-integral K-BKZ fluid, expressing the Weissenberg number *We* versus the eccentricity ε.

Weissenberg number $We = 2.0$ for $\varepsilon = 0.1$ and two angular sections ($\theta = \Phi = 0$ and $\theta = \Phi = \pi$). The curves reveal significant differences between the three fluids, notably for the K-BKZ fluid at $\theta = \Phi = 0$, the angle of the smallest gap between the two cylinders. These observations can be related to differences in the behaviour of the K-BKZ and Oldroyd-B or Maxwell fluids. In terms of the velocity gradient, the viscosity of both differential models is a constant but decreases for the memory-integral fluid.

5.2. Numerical procedure for mixed regime flows with local transformations

Such situations make it necessary to consider local transformations and domain decomposition. Referring to previous results concerning flows in the annulus of cylinders where inertial effects are ignored [30], we adopted two elementary sub-domains Ω_1 and Ω_2 for the applications such that $\Omega = \Omega_1 \cup \Omega_2$, as shown in Figure 7(a). The angle θ_1 corresponds to the limiting section between sub-domains Ω_1 and Ω_2 and is *a priori* unknown. Two reference kinematic functions ϕ_1 and ϕ_2 are considered at the reference sections $\theta = 0$ and $\theta = \pi$, respectively. For these sub-domains, we define two local transformations $T_i : \Omega_i^* \to \Omega_i$ $(i = 1, 2)$, where $M^*(s, R) \to M(r, \theta)$. The mapped sub-domains Ω_1^* and Ω_2^*, are illustrated in Figure 7(b). The first sub-domain Ω_1 involves only open streamlines. For sub-domain Ω_2, open and closed streamlines can be considered. According to the situation depicted in Figure 2, simple meshes may be defined in the mapped computational domains. Figures 7(a) and 7(b) also depict the

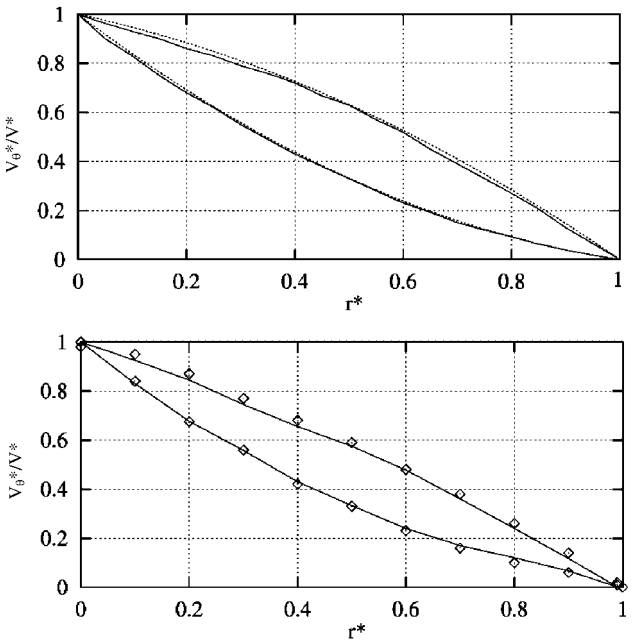

Figure 5. Comparisons of normalized velocity profiles v_θ versus the normalized radial co-ordinate r^* for $\varepsilon = 0.25$, $\theta = \Phi = 0$ and $\theta = \Phi = \pi$, $\omega_0 = 5.2$ rad/s: (a) Newtonian fluid: ——: present work, · · · · ·: lubrication theory (after Berker *et al.* [10]); (b) Carreau fluid: ——: present work; ♢: experimental data from Berker *et al.* [10].

boundary conditions for the physical domain Ω and mapped domains Ω_1^* and Ω_2^* where the mapped streamlines are normalized for computational purposes. The procedure to be followed here for computing the flow characteristics is essentially related to domain decomposition methods, requiring the compatibility equations to be written at the interfaces of the sub-domains. The solution in the total domain Ω should be obtained by considering local sub-problems stated on the sub-domains Ω_i.

The basic ideas for solving the problem can be summarized as follows:

The geometrical domain Ω of boundary Γ is divided into two sub-domains Ω_i $(i = 1, 2)$. Γ_1 denotes the interface of Ω_1 and Ω_2.

If p_i corresponds to the restriction of the pressure p to Ω_i, we may consider local transformations $\alpha_i(s, R)$ and $\beta_i(s, R)$ that verify

- the kinematic equation (38),
- the dynamic equations (39)–(40),
- the following boundary condition equations on $\Gamma \cap \Omega_i$,

$$\begin{aligned} &a_j(\alpha_i, \beta_i, \gamma_i, p_i) = 0 \ (j = 1, 2) \\ &b_j(\alpha_i, \beta_i, \gamma_i, p_i) = 0 \ (j = 1, 2) \\ &p_i = \pi_i \end{aligned} \tag{70}$$

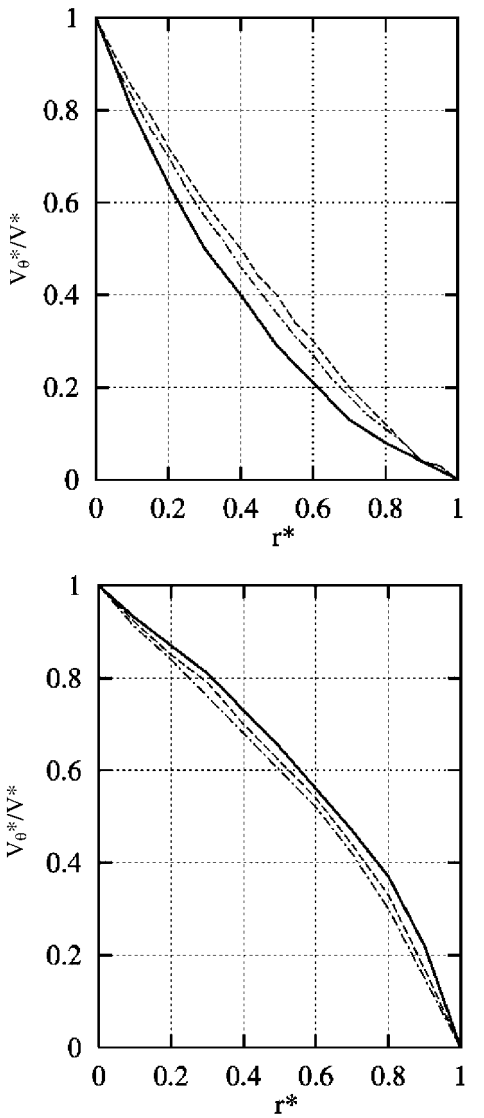

Figure 6. Normalized velocity profiles v_θ versus r^* for Maxwell (- - -), Oldroyd-B (- · - · - ·) and K-BKZ (_____) fluids at $We = 2.0$ ($\varepsilon = 0.1$): (a) $\theta = \Phi = 0$; (b) $\theta = \Phi = \pi$.

- the compatibility conditions at the common boundary Γ_1 of the sub-domains Ω_1 and Ω_2, such that

$$p(M_1^*) = p(M_2^*), \quad \mathbf{V}(M_1^*) = \mathbf{V}(M_2^*) \text{ on } \Gamma_1 \tag{71}$$

where $M_1^* \in \Omega_1$, $M_2^* \in \Omega_2$, with $r(M_1^*) = r(M_2^*)$, $\theta(M_1^*) = \theta(M_2^*)$ on Γ_1.

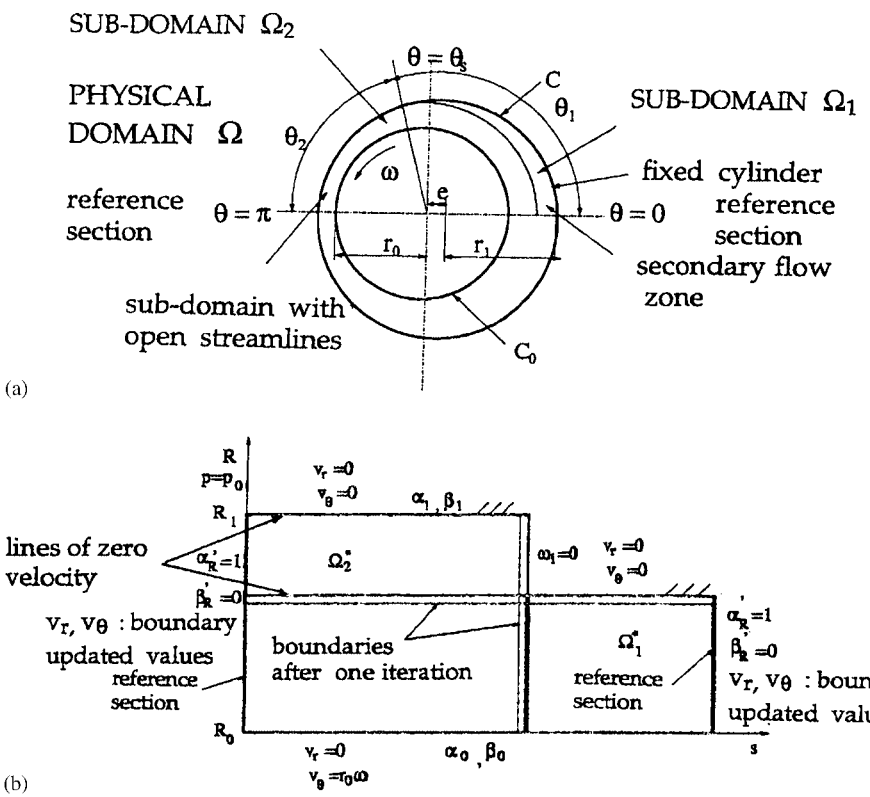

Figure 7. (a) Physical domain Ω partitioned into sub-domains Ω_1 and Ω_2; (b) mapped sub-domains Ω_1^* and Ω_2^* involving boundary conditions.

As pointed out previously, for every sub-domain Ω_i, we consider a reference section S_i to which corresponds a kinematic function ϕ_i, *a priori* unknown.

To solve the problem, the main features of the algorithm can be written according to the following process, given a numerical procedure for solving the equations, upon convergence criteria:

(i) *Initialization*: Definition of the sub-domains Ω_1 and Ω_2; choice of the reference sections S_1 and S_2.
A geometrical shape of the streamlines is assumed, as also the kinematic function $\phi_{i[0]}$ in every mapped sub-domain Ω_i^*, related to the reference section S_i. The initial guess of the streamlines corresponds to an estimate of the local functions α_i and β_i.

(ii) Solve the following set of equations involving the kinematic equation (38), the dynamic equations (39)–(40) and boundary conditions (70)–(71) in the total flow domain Ω^*.

As for global transformations, we still used the Levenberg–Marquardt optimization algorithm to solve the set of governing equations. In the Newtonian case, the initial estimates of the separation angle θ_1 between the sub-domains Ω_1 and Ω_2 and of the kinematic function to be defined at the reference sections were given by the lubrication theory [7]. The size of

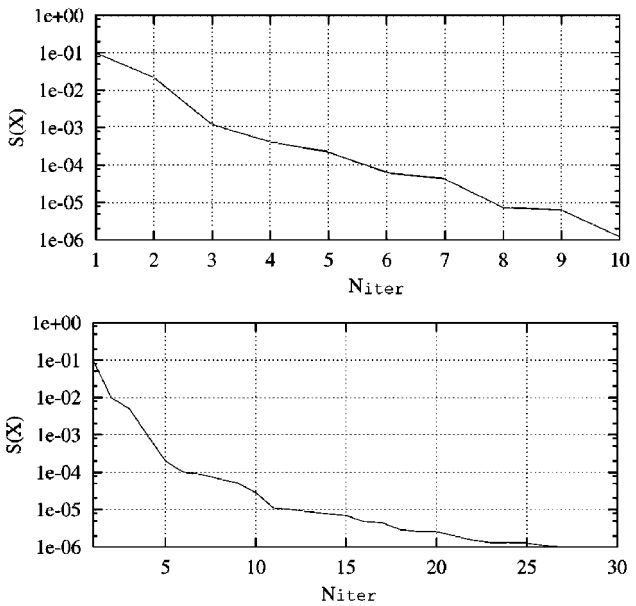

Figure 8. Change in the norm of the objective function versus the iteration number in mixed flow regimes: (a) Newtonian fluid; (b) Memory-integral K-BKZ fluid.

the computational sub-domains is expected to change during the iterations in relation to the moving positions of the separating angle between the two domains. For the non-Newtonian fluids we used as initial estimates the computed Newtonian results. The change in the norm of the objective function $S(\mathbf{X})$ versus the iteration number N_{iter} for the Newtonian and the viscoelastic K-BKZ fluid in the same geometry, shown in Figures 8(a) and 8(b), indicates a lower number of iterations before convergence for the Newtonian fluid. However, satisfactory convergence in obtained in both cases. Our simulations concerned various geometries and flow conditions corresponding to different rotation rates of the moving cylinder. The assumption of flow symmetry was validated by considering firstly the total domain ($0 \leqslant \theta \leqslant 2\pi$) between the eccentric cylinders in our preliminary calculations, thus leading us to reduce the domain of investigation such that $0 \leqslant \theta \leqslant \pi$. In these latter conditions the number of equations and unknowns was approximately 1000.

5.2.1. Comparisons for Newtonian and viscoelastic differential fluids. Figure 9 presents, for a large gap between the eccentric cylinders ($r_0 = 15$ mm, $r_1 = 30$ mm, $e = 7.5$ mm, with a rotation rate $\omega = 250$ rad/s), our numerical results (solid lines) for the streamlines, compared to those previously obtained by Kelmanson [35]. Close agreement between the results may be observed. An example of consistent comparisons with data from Berker *et al.* [10] is given in Figure 10 for the normalized velocity profiles v_θ ($r_0 = 29.9$ mm, $r_1 = 30.3$ mm, $\varepsilon = 0.5$, $\omega = 5.2$ rad/s) at the azimuthal sections $\theta = 0$ and π. However, some discrepancy can be observed in Figures 11(a) and 11(b) for comparisons with data from Beris *et al.* [12], related to the normalized velocity profiles v_r in a journal bearing flow situation, at the azimuthal sections $\theta = \pi/2$ ($r_0 = 30.0$ mm, $r_1 = 33.0$ mm, $\varepsilon = 0.4$) for $We = 2$ and 4, respectively.

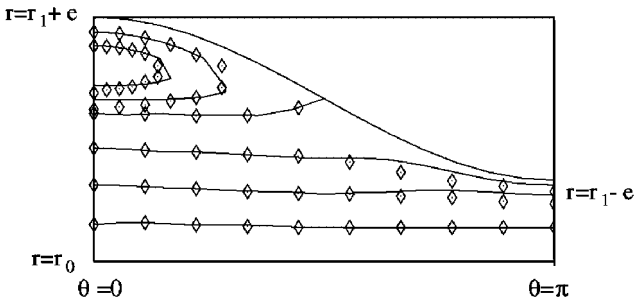

Figure 9. Computational results for the streamlines (Newtonian fluid): ——: present work. ♢: Kelmanson data [35]. The geometrical parameters are: $r_0 = 15\,\text{mm}$, $r_1 = 30\,\text{mm}$, $e = 7.5\,\text{mm}$. The inner cylinder rotates at $\omega = 250\,\text{rad/s}$.

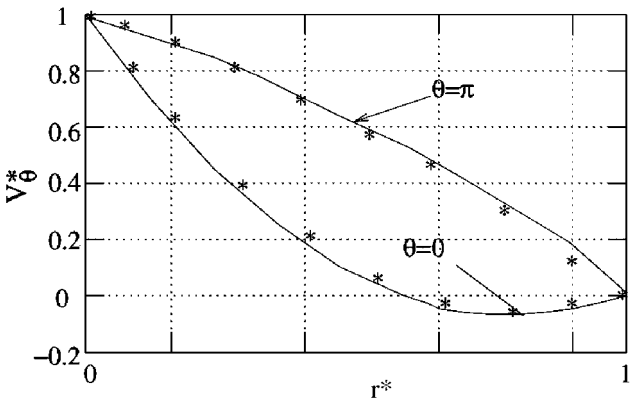

Figure 10. Comparisons between normalized velocity profiles v_θ for $\varepsilon = 0.5$, $\omega = 5.2\,\text{rad/s}$ at the azimuth sections $\theta = 0$ and $\theta = \pi$ for a Newtonian fluid: – – –: present work, ∗ ∗ ∗: results from Berker *et al.* [10] (Newtonian fluid).

Table II. Limit numbers $Re_{\max}$, $We_{\max}$ and E corresponding to journal bearing geometries denoted by $A1$, $A2$, $A3$ and $A4$ (K-BKZ memory-integral fluid).

Geometry	r_0(mm)	r_1(mm)	ε	$\omega_{\max}$(rad/s)	$Re_{\max}$	$We_{\max}$	$E = We/Re_{\max}$
$A1$	29.9	30.3	0.4	6.6	42	25	5.95
$A2$	29.9	30.3	0.5	9.1	58	35	6.03
$A3$	29.9	30.3	0.6	6.6	42	25	5.95
$A4$	29.9	30.3	0.7	3.9	25	15	6.00

5.2.2. Memory-integral viscoelastic fluid. Various geometries and flow conditions corresponding to different Reynolds and Weissenberg numbers were considered when using the viscoelastic K-BKZ fluid. In conditions of journal bearing flows, the limiting Reynolds and Weissenberg values attained before divergence of the algorithm were found to depend on the eccentricity, as shown in Table II. It may be observed that the minimum limit values of *Re* and *We* are

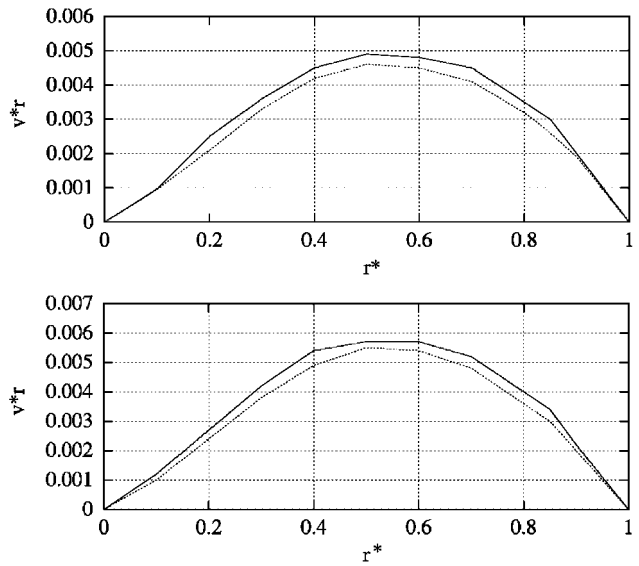

Figure 11. Comparisons with data from Beris *et al.* [10], for normalized velocity profiles v_r in a journal bearing geometry at the azimuth section $\theta = \pi/2$ ($r_0 = 30.0$ mm, $r_1 = 33.0$ mm, $\varepsilon = 0.4$) for (a) $We = 2$ and (b) $We = 4$ (Maxwell fluid).

obtained for the maximum eccentricity between the cylinders. The limit ratio $E = We/Re_{\max}$ of Table II is found to be practically a constant. For the same Weissenberg number ($We = 10$), Figures 12(a)–(c) presents streamline contours for different eccentricities ($\varepsilon = 0.4, 0.5, 0.7$) under journal bearing conditions. The plots of the streamlines indicate an increase of the recirculating flow region with growing eccentricity. The stresses computed with this constitutive equation are given for $\theta = 0$ (maximum gap between the cylinders) in Figure 13, for the $T^{r\theta}$ stress component. It should be underlined that for the Newtonian fluid, this stress component vanishes and there is no recirculation in this case with this model. The shear component $T^{*r\theta}$ does not behave monotonically with respect to the Weissenberg number and the normalized co-ordinate r^*. Such results point to the complexity of the predicting fluid behaviour in journal bearing conditions, in relation to viscoelasticity.

In conditions of journal bearing geometries related to lubrication problems, it is of interest to evaluate the torque C on the inner cylinder of radius r_0, given by

$$C = -(r_0)^2 \int_0^{2\pi} T^{*r\theta}|_{r=r_0}\, \mathrm{d}\theta \tag{72}$$

For the K-BKZ equation, using a dimensionless factor C_0 (chosen as $C_0 = 10$ N (see Reference [23]), the change in torque versus the Weissenberg number We, in conditions corresponding to different eccentricities of the geometries $A1$, $A2$ and $A3$ (Table II) are given in the range 0–6 of We (Figure 14(a)) and, with higher values, up to $We = 30$ (Figure 14(b)). It may be observed that with small values, the torque is a growing function of We and, with higher values of We, it is found to decrease versus We. These results also point to the complex behaviour of viscoelastic fluids used in journal bearing conditions.

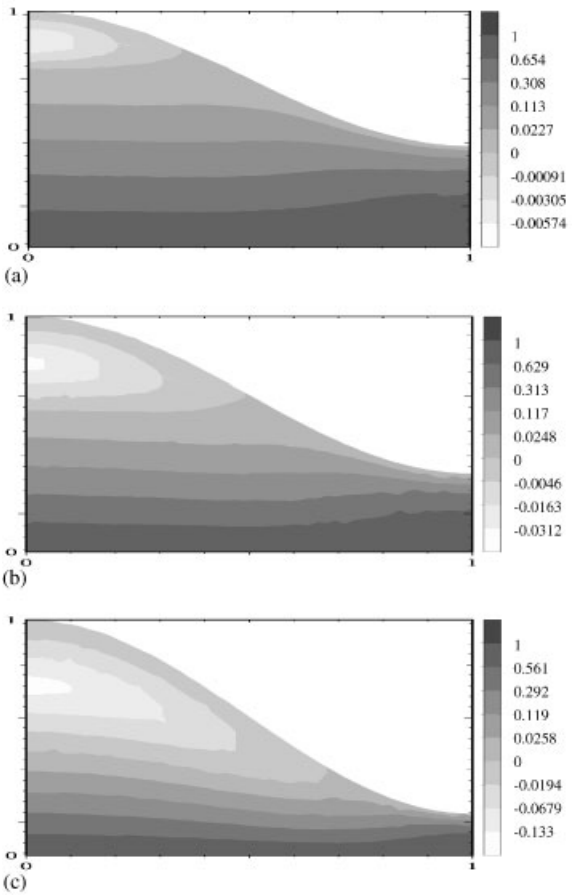

Figure 12. Computed streamlines in a journal bearing geometry ($r_0 = 29.9$ mm, $r_1 = 30.3$ mm) for different eccentricities at the same Weissenberg number $We = 10.0$, with the K-BKZ fluid: (a)$\varepsilon = 0.4$; (b) $\varepsilon = 0.5$; (c) $\varepsilon = 0.7$ (the plots are not to scale).

6. CONCLUSIONS

The formulation presented in this paper has provided a unified approach for the simulation of complex flows involving open streamlines, closed streamlines or both situations, by using global or local transformations and domain decomposition. The flow characteristics are determined by means of unknown transformation functions defined on a mapped computational domain. The automatic verification of mass conservation from the basic equations and the fewer difficulties in particle tracking related to constitutive equations with history-dependence are significant advantages of the approach that deserve to be underlined. Applications to flow calculations in annular geometries between eccentric cylinders, for different classes of fluids, have validated the method by consistent comparisons with existing data from the literature. In addition, some interesting results have been presented, concerning notably:

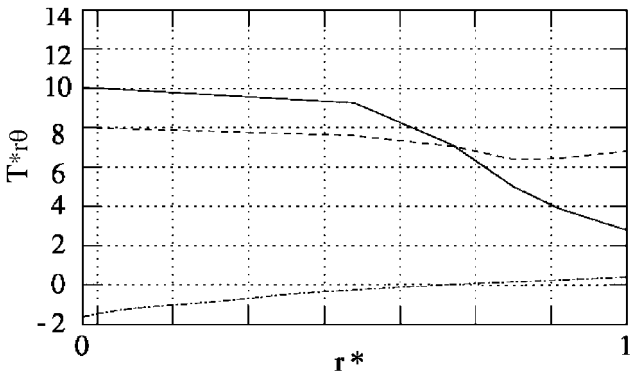

Figure 13. Change in the normalized stresses $T^{*r\theta}$ versus r^* for $We = 0$ (Newtonian fluid), $We = 5$ and 10, with geometry $A2$ of Table I ($\varepsilon = 0.5$) using the memory-integral constitutive equation at the azimuthal section $\theta = 0$.

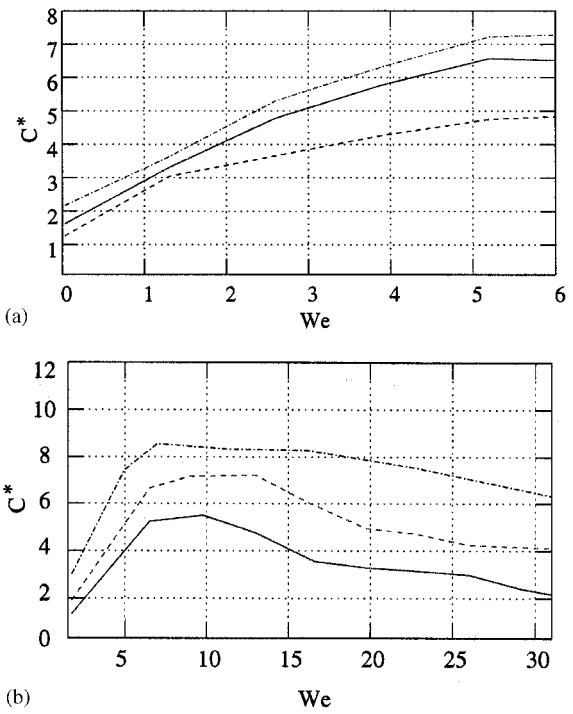

Figure 14. Changes in the torque versus *We* for different eccentricities (geometries $A1$, $A2$ and $A3$) with the memory-integral K-BKZ equation: (a) range 0–6 of *We*: - - -: $\varepsilon = 0.4$; —: $\varepsilon = 0.5$; · ·: $\varepsilon = 0.6$; (b) higher values of *We*: – – –: $\varepsilon = 0.4$; - - -: $\varepsilon = 0.5$; · - · - · -: $\varepsilon = 0.6$.

- the appearance of recirculation, that is related to the limit of convergence of the algorithms based on global transformations;
- for the first time, to our knowledge, numerical results with a realistic K-BKZ memory-integral constitutive equation. Particularly, the numerical predictions with this model have pointed out that flows of polymers associated with lubrication processes are extremely complex to describe.

REFERENCES

1. Diprima RC, Stuart JT. Non-local effects in the stability of flow between eccentric cylinders. *Journal of Fluid Mechanics* 1972; **54**:393–415.
2. Ballal BY, Rivlin RS. Flow of Newtonian fluid between eccentric rotating cylinders: inertia effects. *Archive for Rational Mechanics and Analysis* 1977; **62**:237–294.
3. San Andres A, Szeri AZ. Flow between eccentric rotating cylinders. *Journal of Applied Mechanics* 1984; **51**: 869–878.
4. Oikawa M, Karasudani T, Funakoshi M. Stability of flow between eccentric rotating cylinders. *Journal of Physical Society of Japan* 1989; **58**:2355–2364.
5. Ramesh PS, Lean MH. A boundary-integral equation for Navier–Sokes equations—application to flow in annulus of eccentric cylinders. *International Journal for Numerical Methods in Fluids* 1991; **13**(3):355–369.
6. Frêne J, Nicolas D, Degueurce B, Berthe D, Godet M. *Lubrification hydrodynamique—Paliers et Butees*. Editions Eyrolles: Paris, 1990.
7. Williamson BP, Walters K, Bates TW, Coy RC, Milton AL. The viscoelastic properties of multigrade oils and their effect on journal-bearing characteristics. *Journal of Non-Newtonian Fluid Mechanics* 1997; **73**:115–126.
8. Phan N, Thien, Tanner RI. Journal lubrification and normal stress measurement. *Journal of Non-Newtonian Fluid Mechanics* 1981; **9**:107–117.
9. Davies AR, Li XK. Numerical modeling of pressure and temperature effects in viscoelastic flow between eccentrically rotating cylinders. *Journal of Non-Newtonian Fluid Mechanics* 1994; **54**:331–350.
10. Berker A, Bouldin MG, Kleis SJ, Van Arsdale WE. Effects of polymer on flow in journal bearings. *Journal of Non-Newtonian Fluid Mechanics* 1995; **56**:333–345.
11. Rh. Gwynllyw D, Phillips TN. Preconditioned iterative method for unsteady non-Newtonian flow between eccentrically rotating cylinders. SIAM *Journal of Scientific Computing* 1996; **17**:1369–1394.
12. Beris AN, Armstrong RC, Brown RA. Finite element calculation of viscoelastic flow in a journal bearing: I. Small eccentricites. *Journal of Non-Newtonian Fluid Mechanics* 1984; **16**:141–172.
13. Beris AN, Armstrong RC, Brown RA. Spectral/finite element calculations of the flow of a Maxwell fluid between eccentric rotating cylinders. *Journal of Non-Newtonian Fluid Mechanics* 1987; **22**:129–167.
14. Chawda A, Avgousti M. Stability of viscoelastic flow between eccentric rotating cylinders. *Journal of Non-Newtonian Fluid Mechanics* 1996; **13**:97–120.
15. Li XK, Rh Gwynllyw D, Davies AR, Phillips TN. On the influence of lubricant properties on the dynamics of two-dimensional journal bearings. *Journal of Non-Newtonian Fluid Mechanics* 2000; **93**:29–59.
16. Papanastasiou AC, Scriven LE, Macosco CW. A finite element method for liquid with memory. *Journal of Non-Newtonian Fluid Mechanics* 1987; **22**:271–288.
17. Luo XL, Tanner RI. A streamline element scheme for solving viscoelastic flow problems—Part II: integral constitutive models. *Journal of Non-Newtonian Fluid Mechanics* 1986; **22**:61–89.
18. Luo XL, Mitsoulis E. An efficient algorithm for strain-history tracking in finite element computations of non-Newtonian fluids with integral constitutive equations. *International Journal for Numerical Methods in Fluids* 1990; **11**:1015–1031.
19. Clermont J-R, De la Lande ME, Pham Dinh T, Yassine A. Analysis of plane and axisymmetric incompressible flows by the stream tube method. Numerical simulation with a trust region optimization algorithm. *International Journal for Numerical Methods in Fluids* 1991; **13**(3):371–399.
20. Clermont J-R, de la Lande ME. Calculation of main flows of a memory-integral fluid in an axisymmetric contraction at high Weissenberg numbers. *Journal of Non-Newtonian Fluid Mechanics* 1993; **46**:89–110.
21. Normandin M, Clermont J-R. Three-dimensional extrusion swell: formulation with the stream tube method and numerical results for a Newtonian fluid. *International Journal for Numerical Methods in Fluids* 1996; **23**(9):937–952.
22. Clermont J-R, Normandin M, Radu D. Some remarks on the concept of stream tubes for numerical simulations of complex fluid flows. Applications. *Control and Cybernetics* 2000; **29**(2):535–554.
23. Radu D. Formulations théoriques et simulations numériques d'écoulements de fluides viscoélastiques. *Ph. D. Thesis*, Institut National Polytechnique de Grenoble, April 2000.
24. Bird RB, Armstrong RC, Hassager O. *Dynamics of Polymer Liquids*. Wiley: New York, 1976.

25. Papanastasiou AC, Scriven LE, Macosco CW. An integral constitutive equation for mixed flows: viscoelastic characterization. *Journal of Rheology* 1983; **27**(4):387–410.
26. Chai MS, Yeow YL. Modelling of fluid M1 using multiple-relaxation-time constitutive equations. *Journal of Non-Newtonian Fluid Mechanics* 1990; **35**:459–470.
27. Adachi K. Calculation of strain histories with Protean co-ordinate systems. *Rheologica Acta* 1983; **22**:326–335.
28. Adachi K. A note on the calculation of strain histories in orthogonal streamline co-ordinate systems. *Rheologica Acta* 1986; **25**:555–563.
29. Duda JL, Vrentas JS. Fluid mechanics of laminar liquid jets. *Chemical Engineering Science* 1967; **22**:855–869.
30. Béreaux Y, Clermont JR. Numerical simulation of non-Newtonian complex flows using the stream-tube method and memory-integral constitutive equations. *International Journal for Numerical Methods in Fluids* 1995; **21**:371–389.
31. Normandin M, Clermont JR, Guillet J, Raveyre C. Three-dimensional extrudate swell. Experimental and numerical study of a polyethylene melt obeying a memory-integral equation. *Journal of Non-Newtonian Fluid Mechanics* 1999; **87**:1–25.
32. Fletcher R. *Practical Methods of Optimization*. Wiley: New York, 1987.
33. Gourdin A, Boumahrat M. Méthodes numériques appliquées, *Technique et Documentation*. Editions Lavoisier: Paris, 1989.
34. Dai R-X, Dong Q, Szeri AZ. Flow between eccentric rotating cylinders: bifurcation and stability. *International Journal of Engineering Science* 1992; **130**:1323–1340.
35. Kelmanson MA. A boundary integral equation method for the study of slow flow in bearings with arbitrary geometries. *Transactions of the ASME* 1984; **108**:260–264.

